Upstream conditions at Mercury during the first MESSENGER flyby: Results from two independent solar wind models

Bertalan Zieger,[1,2] Kenneth C. Hansen,[1] Ofer Cohen,[1,3] Tamas I. Gombosi,[1] Thomas H. Zurbuchen,[1] Brian J. Anderson,[4] and Haje Korth[4]

[1] The primary goal of this paper is to provide estimates of upstream solar wind plasma conditions at Mercury during the January 2008 MESSENGER flyby, based on two completely independent solar wind models. The first is a steady-state three-dimensional (3-D) magnetohydrodynamic (MHD) model of the solar corona and inner heliosphere, which simulates the solar wind propagation from the source surface outward to Mercury, using synoptic charts of the photospheric magnetic field as input. The second model is a time-dependent 1-D MHD model of solar wind propagation that employs actual solar wind data at 1 AU as boundary conditions and propagates the solar wind backward in time to Mercury. We compare and validate the two models with each other as well as with actual magnetic field data from the MESSENGER Magnetometer instrument. Our combined method can produce the most accurate results for the solar wind speed and the sector structure of the interplanetary magnetic field. **Citation:** Zieger, B., K. C. Hansen, O. Cohen, T. I. Gombosi, T. H. Zurbuchen, B. J. Anderson, and H. Korth (2009), Upstream conditions at Mercury during the first MESSENGER flyby: Results from two independent solar wind models, *Geophys. Res. Lett.*, *36*, L10108, doi:10.1029/2009GL038346.

1. Introduction

[2] The knowledge of upstream solar wind conditions at Mercury is essential not only for modeling the planet's magnetosphere-exosphere-surface system but also for interpreting in situ observations inside the magnetosphere. The recent flyby of Mercury by the MErcury Surface, Space ENvironment, GEochemistry, and Ranging (MESSENGER) spacecraft resulted in very exciting measurements and discoveries. Among these were the measurements by the Fast Imaging Plasma Spectrometer (FIPS) sensor on the Energetic Particle and Plasma Spectrometer instrument of ions that must have originally come from the surface of the planet [*Zurbuchen et al.*, 2008]. This ion population may originate directly from the surface via the sputtering process or from a neutral exosphere close to the planet, undergoing energization through the ion pick-up process in either case.

Kabin et al. [2008] pointed out that solar wind access to the surface of Mercury depends strongly on solar wind conditions and therefore these conditions strongly influence the effect of pick-up ions on the global structure of the magnetosphere. For this reason, and due to the fact that the MESSENGER plasma instruments cannot see the solar wind, we intend to provide upstream solar wind conditions at Mercury to the entire MESSENGER community. We do this using a combination of two independent magnetohydrodynamic (MHD) models: the synoptic solar wind model and the reverse propagation model described in Sections 2.1 and 2.2, respectively. We discuss and validate the predictions of the two models in Section 3 and review the advantages and limitations of these modeling approaches in Section 4.

2. Methods

2.1. Synoptic Solar Wind Model

[3] The synoptic solar wind model is a global three-dimensional (3-D) MHD model of the solar corona and the inner heliosphere combined with an empirical solar wind model, which takes into account the coronal heating by means of a variable polytropic index [*Cohen et al.*, 2007]. The model is implemented by coupling these components within the Space Weather Modeling Framework (SWMF) [*Tóth et al.*, 2005]. In order to model the coronal heating, *Cohen et al.* [2007] implement a method that uses the Wang-Sheely-Arge empirical solar wind model [*Arge and Pizzo*, 2000; *Arge et al.*, 2003, 2004] and the Bernoulli equation to relate the final solar wind speed with the photospheric value of the polytropic index along a potential field line, resulting in a variable polytropic index that mimics the volumetric heating in the corona. A steady-state self-consistent solution of the 3-D MHD equations is obtained in the heliographic rotating frame (HGR). The inner boundary conditions are derived, with the necessary additional assumption of the potential field approximation, from synoptic charts of the photospheric magnetic field observed by the Michelson Doppler Imager (MDI) on board the Solar and Heliospheric Observatory (SOHO) spacecraft. The synoptic solar wind model has been validated against solar wind observation at 1 AU, using a full year of Advanced Composition Explorer (ACE) and Wind spacecraft data during solar minimum as well as during solar maximum [*Cohen et al.*, 2008]. It was shown that the model predicts the magnitude of the solar wind plasma variables, namely speed, density, and temperature, reasonably well on a large scale irrespective of the transients that cannot be simulated with a steady-state model. Different magnetograms sources provide similar distribution of the

---

[1]Department of Atmospheric, Oceanic and Space Sciences, University of Michigan, Ann Arbor, Michigan, USA.

[2]Also at Geodetic and Geophysical Research Institute, Hungarian Academy of Sciences, Sopron, Hungary.

[3]Now at Harvard-Smithsonian Center for Astrophysics, Cambridge, Massachusetts, USA.

[4]Johns Hopkins University Applied Physics Laboratory, Laurel, Maryland, USA.

photospheric magnetic field. However, they are sometimes inconsistent in their magnitude. Due to this discrepancy and due the lack of our potential field based MHD model to capture open flux that originates from active regions [*Cohen et al.*, 2008], we use a scaling factor for the input magnetogram. The scaling factor is an additional free parameter that enables us to obtain the best fitting solution at 1 AU, which we do on a case-by-case basis. This results in the best possible solar wind predictions at Mercury. In the present paper we use the MDI synoptic chart for Carrington Rotation 2065 as input for the 3-D steady-state simulation. The MHD solution was extracted along the trajectory of MESSENGER in the vicinity of the January 2008 Mercury flyby. Although the grid resolution gradually decreases with the heliocentric distance, the adaptive mesh refinement technique (AMR) applied in the 3-D MHD code gives a spatial resolution as high as 0.2 solar radii close to the heliospheric current sheet at 0.3 AU.

2.2. Reverse Propagation Model

[4] Recently a 1-D MHD model of solar wind propagation, now known as the Michigan Solar Wind Model (MSWiM, http://mswim.engin.umich.edu/), has been developed and sufficiently validated on a statistical basis against 12 years of heliospheric solar wind data from the Pioneer, Voyager, and Ulysses spacecraft [*Zieger and Hansen*, 2008]. This model uses near-Earth solar wind observations as time-dependent boundary conditions at 1 AU and propagates the solar wind outward in the heliosphere up to 10 AU. The 1-D ideal MHD equations are solved in the inertial frame along a line in the ecliptic at a selected helioecliptic longitude with spherical symmetry in the perpendicular directions. The boundary conditions at 1 AU are rotated from the Earth to the simulation longitude under the assumption that the solar corona is in quasi-steady state on time scales of half a solar rotation. A similar rotation procedure is applied to rotate the MHD solution to planets, spacecraft, or any other moving celestial body. As a recent application of MSWiM, propagated solar wind data have been used to facilitate the interpretation of Jovian and Kronian aurora observations during the four Hubble Space Telescope (HST) campaigns in 2007 and 2008 [*Bunce et al.*, 2008; *Clarke et al.*, 2009]. For further details on the numerical method underlying MSWiM, the reader is referred to the papers by *Zieger and Hansen* [2008] and *Tóth* [1996]. We have adapted MSWiM for reverse propagation of the solar wind backward in time, which is then applied to estimate upstream solar wind conditions at Mercury from near-Earth observations. Technically, the reverse propagation from Earth to Mercury is implemented with a standard forward propagation in a numerical sense, where the simulation time runs forward (positive time step), but the actual boundary conditions at 1 AU, where the radial flow velocity has been reversed, are fed in the model in a time-reversed manner. The geometry of the simulation also changes in that now the solar wind propagates from the outer boundary (1 AU) towards the inner boundary (0.3 AU), undergoing compression and deceleration rather than expansion and acceleration. In the final step of the simulation, the simulation time is converted back to real time to obtain the desired time series of the eight MHD variables at Mercury or MESSENGER. Another implemen-

tation of the reverse propagation would have been to reverse the time step (negative time step) in a forward propagation from 0.3 to 1 AU, but this option had to be excluded because the numerical methods for solving the MHD equations are known to be unstable for negative time stepping. In either case, an inward propagation in principle violates the basic physical principal of irreversibility of entropy variations at interplanetary shocks. However, steep shock structures tend to form farther out in the solar wind than the orbit of Mercury (and often Earth) so it was hoped that the reverse propagation would work reasonably well. As a validity test of the reverse propagation, we performed an additional forward propagation from 0.3 AU to Earth using the simulated solar wind conditions at Mercury as input boundary conditions. The solar wind propagated back to Earth in this way was found to be practically identical with the original solar wind input. If the irreversibility of entropy variations at shocks was an issue, the original solar wind data and the doubly propagated model solar wind would not have been the same. In these simulations, we used hourly solar wind plasma and interplanetary magnetic field (IMF) data from the OMNI 2 database (http://omniweb.gsfc.nasa.gov/html/omni2_doc.html) in RTN coordinates, and consequently the output solar wind data at Mercury or MESSENGER are obtained in the same coordinate system with a comparable temporal resolution. The RTN system is centered at a spacecraft or planet and oriented with respect to the line connecting the Sun and spacecraft or planet. The R (radial) axis is directed radially away from the Sun through the spacecraft or planet. The T (tangential) axis is the cross product of the Sun's spin vector and the R axis, and the N (normal) axis completes the right handed set. As a final note, we point out that the radial magnetic component cannot change in time in 1-D MHD simulations because of the $\nabla \cdot \mathbf{B} = 0$ constraint, so we are not able to predict this magnetic component at Mercury with the reverse propagation model.

3. Results and Validation

[5] We extracted the MHD solution, i.e., the time series of the eight MHD variables, three vector components of the velocity (v_R, v_T, v_N), three vector components of the magnetic field (B_R, B_T, B_N), plasma density (ρ), and plasma temperature (T), from the two completely independent simulations described in Sections 2.1 and 2.2 along the trajectory of MESSENGER in a time window centered on the date of the January 14, 2008, Mercury flyby. We also extracted the MHD solution at Mercury (not shown in this paper), which was practically identical with that at MESSENGER at the time of the encounter due to the grid resolution. Nevertheless, we present the results for the MESSENGER trajectory here to allow direct comparison with MESSENGER observations. The solar wind plasma variables obtained from the two different models are compared in Figure 1. We find the best agreement between the two models for the radial velocity. This is consistent with our previous validation results, which show that this quantity is the most accurately modeled [*Zieger and Hansen*, 2008]. The radial velocity curves (Figure 1, top) clearly show that MESSENGER passed a high-speed solar wind stream (exceeding 600 km/s) while approaching Mercury,
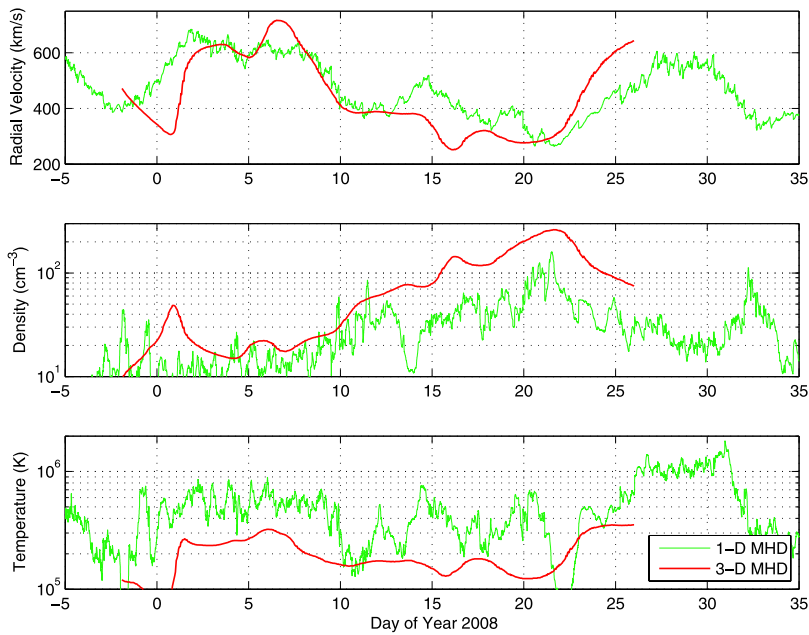
Figure 1. Solar wind plasma variables at MESSENGER predicted by the two independent MHD models. The green line indicates the 1-D reverse propagation model results, while the red line indicates the results from the 3-D synoptic solar wind model.

and it entered the slow-speed streamer belt region about 5 days before the encounter. Just before the encounter, the 1-D model indicates a sudden drop in density and a short-lived increase in the speed up to 500 km/s, which is either smoothed out or not captured in the 3-D steady-state model. After the Mercury flyby the density continued to increase and peaked on DOY 22 (Figure 1, middle), after which MESSENGER left the streamer belt and entered a high-speed solar wind stream again. The predicted densities from the two models are comparable in magnitude and similar in their trends (Figure 1, middle), which suggests that the large scale streamer belt structure is relatively well captured in the two models. The largest discrepancy, about a factor of 3, was found between the plasma temperatures of the two models (Figure 1, bottom). This means that with the current physical approximations involved in our models, this plasma parameter can be predicted the least accurately, as also concluded recently by *Zieger and Hansen* [2008]. Comparing the plasma parameters from the two models with the FIPS data (not shown) results in reasonable agreement.

[6] Here we use the magnetic field observations of MESSENGER's Magnetometer (MAG) instrument to validate our MHD models. The predicted IMF magnitude and the three IMF vector components are plotted along with the corresponding hourly averaged MAG data in Figure 2. As mentioned above, the temporal variation of the radial component (B_R) cannot be simulated in the 1-D model because of the $\nabla \cdot \mathbf{B} = 0$ constraint, which is rather unfortunate since this is the dominant IMF component at Mercury due to the small winding angle of the Parker spiral at this heliocentric distance. Luckily enough, B_R is the most reliable magnetic component in the 3-D steady-state model. In fact, the magnetic field at the source surface is assumed to be purely radial in the potential field model. The fit between the predicted B_R from the 3-D model and the actual

MAG data is indeed impressive (see Figure 2b). Heading towards Mercury, MESSENGER crossed the heliospheric current sheet on the last day of 2007, evidenced by the reversal of B_R from negative to positive and by the simultaneous reversal of B_T from positive to negative in the MAG data, which is precisely reproduced by the 3-D model. Until the encounter with Mercury, MESSENGER stayed in the away IMF sector (positive B_R and negative B_T) and the IMF magnitude gradually increased due to the decreasing heliocentric distance of the spacecraft (Figure 2a). Shortly after the Mercury flyby, between DOY 15 and 16, MESSENGER crossed the heliospheric current sheet again, now entering the toward IMF sector, which is again perfectly matched with the corresponding reversal of B_R and B_T (Figures 2b and 2c) and the sudden drop of the magnetic field intensity (Figure 2a) predicted by our 3-D model. This current sheet crossing is also supported by the plasma variables in that the speed has a local minimum and the density has a local maximum exactly at the time of the reversal of the magnetic field vector (see Figure 1). On DOY 20 and 21, MESSENGER experienced another period of suddenly decreased magnetic filed intensity (as low as 10 nT) accompanied by repeated reversals of B_R and B_T. Even this short observed dropout of the magnetic field is relatively well reproduced by our 3-D model (Figure 2a). The authors would like to point out here that both MHD models predict the highest density and the lowest speed in this particular time interval (Figures 1, middle and 1, top), which implies that MESSENGER may have returned temporarily to the heliospheric plasma sheet. Although the reverse propagation model gives reasonable estimates for B_T and B_N in the middle of IMF polarity sectors, it apparently fails in periods of multiple current sheet crossings (green curves in Figure 2). This can be attributed to the above-mentioned $\nabla \cdot \mathbf{B} = 0$ constraint in 1-D MHD, which does not allow
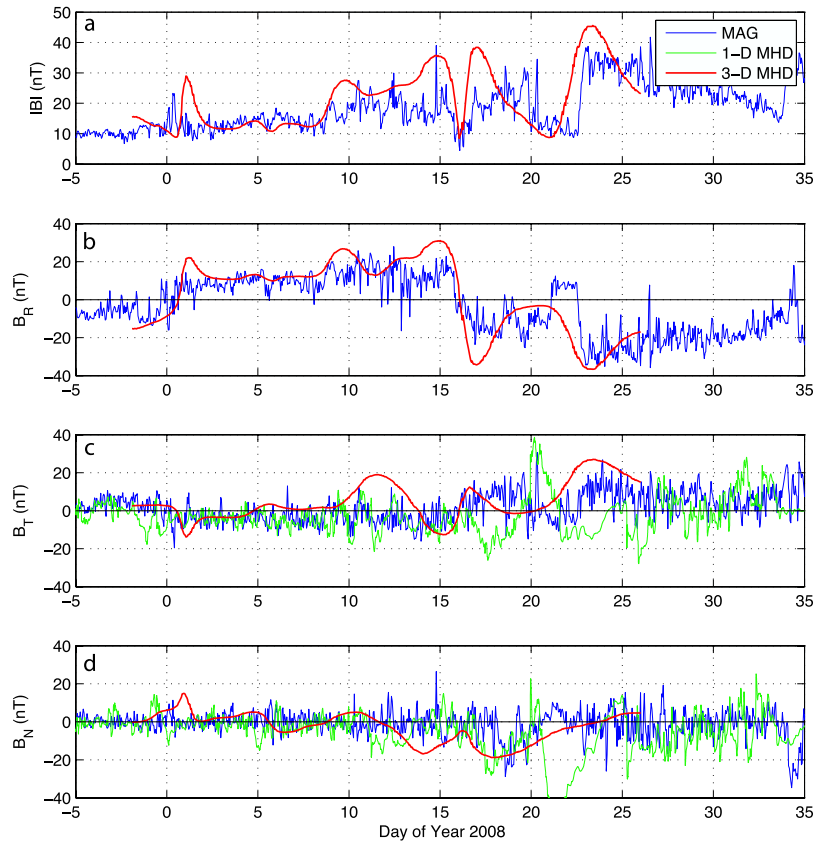
Figure 2. Predicted and observed IMF magnitude and IMF vector components at MESSENGER. The green line indicates the 1-D reverse propagation model results, the red line indicates the results from the 3-D synoptic solar wind model, and the blue line represents the actual MESSENGER MAG observations.

the reversal of B_R in the simulation. This numerical problem could be resolved only in a 2-D reverse propagation model, which would give time-dependent predictions also for the radial IMF component.

4. Conclusions

[7] We have provided estimates of upstream solar wind conditions at Mercury in a time window of about one Carrington Rotation around the January 2008 MESSENGER flyby on the basis of two completely independent models: a synoptic solar wind model and a reverse propagation model described in Sections 2.1 and 2.2. Although the latter approach is a novel way of simulating the solar wind, the method is well tested. We first tested the reversibility of the method by propagating the simulation results at Mercury back to Earth (forward in time). The back- and forward-propagated solar wind at Earth was found to be practically identical to the original input, indicating that the backward propagation does not result in problems with conservation. As a second test, we compared results from the two models. Finally we validated both models with actual magnetic field data from the MESSENGER MAG instrument. The specific advantages and limitations of the two models are fortunately complementary to each other in some respects. The spatial (and hence temporal) resolution of the synoptic solar wind model is limited because of the huge size of the 3-D simulation box extending from the source surface to 1 AU, in contrast to the 1-D reverse propagation model, which is

relatively inexpensive even for highly increased spatial resolution. The reverse propagation model is driven by time-dependent boundary conditions at 1 AU, which can capture even transient events close to the times of Sun-Mercury-Earth alignment, whereas the synoptic model provides a steady-state solution for the global structure of the 3-D inner heliosphere excluding short-lived transients. The reverse propagation model employs actually measured solar wind data at 1 AU as input boundary conditions, while the synoptic model needs to make a significant amount of approximation to derive solar wind boundary conditions at the source surface from photospheric magnetic field observations. Moreover, since the physics involved in the acceleration of the solar wind is still unknown, the synoptic model incorporates an empirical solar wind model to simulate volumetric heating in the corona by means of a variable polytropic index. Because of the uncertainties involved in the potential field model, the magnitude of the magnetic field component in the synoptic model needs to be scaled to fit observations at 1 AU. The 1-D reverse propagation model is limited to radial plasma interactions exclusively, for spherical symmetry in the perpendicular directions, as opposed to the synoptic model that solves the 3-D MHD equations self-consistently. Because of the $\nabla \cdot \mathbf{B} = 0$ constraint, the radial magnetic field (B_R) is not allowed to change in time in the 1-D MHD model, unlike in the fully 3-D MHD model. The latter is one of the main advantages of the synoptic model, since at Mercury, B_R is the dominant magnetic

component carrying important information on the interplanetary sector structure. The adiabatic reverse propagation model has been found to be reversible, hence isentropic at least in the heliocentric ranges between Mercury and Earth, whereas the synoptic model allows for irreversible entropy variations through a variable polytropic index. The combined application of these two independent solar wind models has the additional advantage of providing approximate error estimates for the predicted solar wind variables, which is valuable information for the users. The authors are convinced that the solar wind predictions at Mercury presented in this paper can facilitate the interpretation of different MESSENGER measurements during the first flyby and support the modeling efforts to describe the global magnetospheric structure of Mercury. The synoptic solar wind model and the reverse propagation model are proven to be efficient tools to determine solar wind conditions in the inner heliosphere that will be used during the coming Mercury flybys and possibly for other inner heliospheric missions as well.

References

Arge, C. N., and V. J. Pizzo (2000), Improvement in the prediction of solar wind conditions using near-real time solar magnetic field updates, *J. Geophys. Res.*, *105*, 10,465–10,479.

Arge, C. N., D. Odstrcil, V. J. Pizzo, and L. R. Mayer (2003), Improved method for specifying solar wind speed near the Sun, in *Solar Wind Ten, Proceedings of the Tenth International Solar Wind Conference*, edited by M. Velli, R. Bruno, F. Malara, and B. Bucci, *Am. Inst. Phys. Conf. Ser.*, *679*, 190–193.

Arge, C. N., J. G. Luhmann, D. Odstrcil, C. J. Schrijver, and Y. Li (2004), Stream structure and coronal sources of the solar wind during the May 12th, 1997 CME, *J. Atmos. Sol. Terr. Phys.*, *66*, 1295–1309, doi:10.1016/j.jastp.2004.03.018.

Bunce, E. J., et al. (2008), Origin of Saturn's aurora: Simultaneous observations by Cassini and the Hubble Space Telescope, *J. Geophys. Res.*, *113*, A09209, doi:10.1029/2008JA013257.

Clarke, J. T., et al. (2009), The response of Jupiter's and Saturn's auroral activity to the solar wind, *J. Geophys. Res.*, doi:10.1029/2008JA013694, in press.

Cohen, O., et al. (2007), A semiempirical magnetohydrodynamical model of the solar wind, *Astrophys. J.*, *654*, L163–L166.

Cohen, O., I. V. Sokolov, I. I. Roussev, and T. I. Gombosi (2008), Validation of a synoptic solar wind model, *J. Geophys. Res.*, *113*, A03104, doi:10.1029/2007JA012797.

Kabin, K., M. H. Heimpel, R. Rankin, J. M. Aurnou, N. Gomez-Perez, J. Paral, T. I. Gombosi, T. H. Zurbuchen, P. L. Koehn, and D. L. DeZeeuw (2008), Global MHD modeling of Mercury's magnetosphere with applications to the MESSENGER mission and dynamo theory, *Icarus*, *195*, 1–15, doi:10.1016/j.icarus.2007.11.028.

Tóth, G. (1996), A general code for modeling MHD flows on parallel computers: Versatile Advection Code, *Astrophys. Lett. Commun.*, *34*, 245–250.

Tóth, G., et al. (2005), Space Weather Modeling Framework: A new tool for the space science community, *J. Geophys. Res.*, *110*, A12226, doi:10.1029/2005JA011126.

Zieger, B., and K. C. Hansen (2008), Statistical validation of a solar wind propagation model from 1 to 10 AU, *J. Geophys. Res.*, *113*, A08107, doi:10.1029/2008JA013046.

Zurbuchen, T. H., J. M. Raines, G. Gloeckler, S. M. Krimigis, J. A. Slavin, P. L. Koehn, R. M. Killen, A. L. Sprague, R. L. McNutt Jr., and S. C. Solomon (2008), MESSENGER observations of the composition of Mercury's ionized exosphere and plasma environment, *Science*, *321*, 90–92, doi:10.1126/science.1159314.

_____

B. J. Anderson and H. Korth, Johns Hopkins University Applied Physics Laboratory, 11100 Johns Hopkins Road, Laurel, MD 20723, USA.

O. Cohen, Harvard-Smithsonian Center for Astrophysics, 60 Garden Street, Cambridge, MA 02138, USA.

T. I. Gombosi, K. C. Hansen, B. Zieger, and T. H. Zurbuchen, Department of Atmospheric, Oceanic and Space Sciences, University of Michigan, 2455 Hayward Street, Ann Arbor, MI 48109, USA. (bzieger@umich.edu)